# Construction and validation of a nomogram for the diagnosis of postmenopausal osteoporosis

LE-YI HUANG[1*], YAO CHEN[1*], LIN-RAN SONG[1*], ZHUO-LIN ZHONG[1], KAMRAN ALI[2], HUI-MIN LI[1], QING-FENG HU[1] and HONG-HUA HU[3]

[1]Department of Orthopedics, The Fourth Affiliated Hospital of School of Medicine and International School of Medicine, International Institutes of Medicine, Zhejiang University, Yiwu, Zhejiang 322000, P.R. China; [2]Department of Surgery, The Fourth Affiliated Hospital of School of Medicine and International School of Medicine, International Institutes of Medicine, Zhejiang University, Yiwu, Zhejiang 322000, P.R. China; [3]Department of Dermatology, The Fourth Affiliated Hospital of School of Medicine, and International School of Medicine, International Institutes of Medicine, Zhejiang University, Yiwu, Zhejiang 322000, P.R. China

Received May 29, 2026; Accepted July 2, 2026

DOI: 10.3892/mmr.2026.13989

**Abstract.** Osteoporosis (OP) is an increasing global public health concern and practical tools for predicting and detecting postmenopausal osteoporosis (PMOP) at an early stage are still needed. The present study aimed to develop and validate an individualized diagnostic prediction model for PMOP to facilitate risk assessment and guide therapeutic strategies for high-risk patients. RNA sequencing data and corresponding clinical features were obtained from the Gene Expression Omnibus database (training group, n=90) and The Fourth Affiliated Hospital of School of Medicine and International School of Medicine, Zhejiang University, Zhejiang China (validation group, n=18). Gene Set Enrichment Analysis (GSEA) and Protein-Protein Interaction (PPI) network analyses were used to identify hub genes associated with OP. Univariate, multivariate, least absolute shrinkage and selection operator logistic regression analyses were performed to identify the factors and generate a dynamic nomogram. Validation was performed using the receiver operating characteristic curve and decision curve analysis (DCA) to evaluate the effectiveness and net benefit of the clinical prediction nomogram. PPI and GSEA identified 13 estrogen-response-related hub genes (CD44, FDFT1, SLC29A1, P2RY2, RHOBTB3, TNNC1, RPS6KA2, TSKU, CYP26B1, SEMA3B, SYT12, IL17RB and ELF3) that were incorporated into a risk score model. A nomogram combining this risk score with clinical parameters demonstrated a promising preliminary diagnostic performance for OP. DCA indicated that the combined risk score and clinical-factor model provided the highest net benefit. The clinical prediction nomogram exhibited a promising preliminary performance in both the training and validation groups. The present study developed a novel diagnostic nomogram for predicting PMOP. This exploratory tool showed potential clinical utility for risk stratification, although prospective validation in larger cohorts is required before clinical application.

*Correspondence to:* Dr Qing-Feng Hu, Department of Orthopedics, The Fourth Affiliated Hospital of School of Medicine, and International School of Medicine, International Institutes of Medicine, Zhejiang University, N1 Shangcheng Avenue, Yiwu, Zhejiang 322000, P.R. China
E-mail: 8021009@zju.edu.cn

Ms. Hong-Hua Hu, Department of Dermatology, The Fourth Affiliated Hospital of School of Medicine and International School of Medicine, International Institutes of Medicine, Zhejiang University, N1 Shangcheng Avenue, Yiwu, Zhejiang 322000, P.R. China
E-mail: drhuhonghua@zju.edu.cn

*Contributed equally

*Abbreviations:* BMD, bone mineral density; BP, biological process; CC, cellular component; DCA, decision curve analysis; DEGs, differentially expressed genes; DXA, dual-energy X-ray absorptiometry; GEO, Gene Expression Omnibus; GO, Gene Ontology; GSEA, Gene Set Enrichment Analysis; GPCR, G protein-coupled receptor; LASSO, least absolute shrinkage and selection operator; MF, molecular function; OP, osteoporosis; PMOP, postmenopausal osteoporosis; PPI, protein-protein interaction; SRP, signal-recognition particle; STRING, Search Tool for the Retrieval of Interacting Genes

*Key words:* osteoporosis, bioinformatics, risk score model, hub gene

## Introduction

Osteoporosis (OP) is a chronic metabolic orthopedic disease characterized by impaired bone strength and increased fracture risk. In China, osteoporotic fractures are projected to reach 4.83 million cases annually by 2035 (1,2). In Europe, an estimated 25.5 million women and 6.5 million men suffered from OP in 2019 (3). Globally, osteoporotic fractures occur in one in two women and one in five men during their lifetime (4). Among OP subtypes, postmenopausal osteoporosis (PMOP)

is the most common and imposes a substantial public health burden because of its high incidence and associated healthcare costs (5,6).

OP often remains asymptomatic until a fragility fracture occurs, which complicates early detection and prevention. Dual-energy X-ray absorptiometry (DXA) is the standard method for assessing bone mineral density (BMD) and osteoporotic fracture risk (7). OP is diagnosed in adults on the basis of an osteoporotic fracture or a T-score ≤-2.5, even when a subsequent DXA T-score exceeds this threshold (8). However, DXA measurements are affected by technical factors, including instrument calibration, patient positioning and analytical methods (9). Additionally, BMD screening requires substantial resources, limiting its accessibility for large-scale screening, particularly in economically disadvantaged regions (10).

Early PMOP screening and risk prediction before marked BMD loss are therefore important for high-risk individuals who may benefit from early interventions to increase peak bone mass, a key determinant of OS and fracture risks (11,12). Calcium and protein intake, together with weight-bearing physical activity, have been shown to help mitigate OP progression (13,14). Early identification of high-risk populations can support preventive strategies that slow bone loss and reduce OP incidence, shifting care from treatment to proactive prevention before measurable BMD deterioration occurs.

Advances in bioinformatics technology have facilitated the analysis of gene expression profiles, disease mechanisms and candidate biomarkers (15,16). Studies have implicated of non-coding RNAs, including microRNAs (miRNAs) and long non-coding RNAs (lncRNAs), as well as proteins, enzymes and hormones, in OP pathogenesis (17-19). High-throughput sequencing combined with bioinformatic analysis offer unprecedented opportunities to identify novel biomarkers and therapeutic targets (20).

Given the need for improved PMOP prediction, it was hypothesized that an effective bioinformatics-based risk model could improve early PMOP diagnosis. The present study aimed to identify potential PMOP biomarkers through bioinformatic approaches and to develop a diagnostic nomogram for risk stratification. The model was further validated by comparing healthy controls and patients with PMOP diagnosed at our hospital.

## Materials and methods

*Database selection*. Gene expression datasets were retrieved from the Gene Expression Omnibus (GEO) database (http://www.ncbi.nlm.nih.gov/geo) to identify studies comparing gene expression profiles between healthy and OP human samples. Only datasets derived from clinical tissue samples were included; animal-model datasets were excluded. The titles and abstracts of the retrieved datasets were screened and datasets of interest were evaluated in detail. GSE 152073 was selected for further analysis. This dataset was generated using the GPL17586 Affymetrix Human Transcriptome Array 2.0 platform and included 46 healthy and 44 OP human samples and was used to develop the risk score model.

*Differential gene expression analysis*. After gene reannotation, differential expression analysis of GSE152073 was performed using the 'limma' R package (21). Differentially expressed genes (DEGs) were selected using |fold change| >1 and an adjusted P-value (False Discovery Rate) <0.05. Duplicate gene entries were averaged. Expression levels were $\log_2$-transformed and quantile-normalized. The top 10 differentially regulated genes were selected for further analysis (22).

*Functional analysis*. Functional enrichment analysis of DEGs was performed using the Search Tool for the Retrieval of Interacting Genes (STRING) database (http://string-db.org/). Gene Ontology (GO) annotation, including biological process (BP), molecular function (MF), cellular component (CC) and Reactome (release 97; https://reactome.org/) pathway enrichment analyses, was conducted to explore the biological significance of the DEGs (23). P<0.05 was considered to indicate a statistically significant difference. The top 10 enriched GO terms and Reactome pathways were downloaded for further analysis. Gene Set Enrichment Analysis (GSEA) was performed to determine the molecular functional pathways (24). The reference gene set file was chosen as 'h.all. v7.4. symbols.gmt', and the enriched pathway-associated genes were extracted for further investigation.

*PPI network*. The STRING database was used to develop a PPI network to identify possible interaction among DEGs (23). PPI node pairs with a medium combined score of 0.4 were selected as significant. The PPI network was visualized using the Cytoscape software (version 3.8.2, www.cytoscape.org/). Network reliability was assessed based on nodes with a high degree of connectivity (25). The CytoHubba plugin tests were used to calculate the degree of connectivity for each protein node in Cytoscape and the top 30 hub genes were visualized. The top 10 highly connected hub genes were selected for further investigation (26).

*Selection of risk-associated genes*. The least absolute shrinkage and selection operator (LASSO) technique, a regression-based analysis tool for penalizing the magnitude of the coefficients of the predictor variables by adding a cap during parameter estimation, was used to select the most appropriate risk genes for PMOP. This method helped reduce the number of variables in the model and the likelihood of overfitting (27). Then 10-fold cross-validation was used for lambda selection and the optimal penalty parameter was chosen as lambda.1se (the largest lambda within one standard error of the minimum cross-validation error) to favor a parsimonious model. Internal validation was performed using bootstrap resampling with 1,000 iterations to obtain the optimism-corrected performance metrics. A uniform shrinkage factor derived from bootstrapping was applied to the model coefficients to correct for overfitting. Model stability was assessed by recording the frequency with which each gene was selected across bootstrap samples; genes retained in >70% of the bootstrap iterations were considered stable predictors.

*Construction of a score model*. A logistic regression analysis model was developed using the risk genes identified using LASSO regression. Model performance was assessed using omnibus tests for coefficients and the Hosmer-Lemeshow test for goodness of fit. P<0.05 was considered to indicate a statistically significant difference. The risk score model was developed

and the risk score was calculated using the following formula: Risk score=$\beta 1$ x $Exp1$ + $\beta 2$ x $Exp2$ + $\beta i$ x $Expi$ + b, where $\beta$ represents the regression coefficient from multiple logistic regression analysis, $Exp$ denotes the gene for expression levels and b is a constant. The predictive performance of the model was evaluated using receiver operating characteristic (ROC) curves and nomograms. A nomogram was constructed to visualize the effect of individual risk factors based on a logistic regression coefficient (28). Calibration curves were generated to assess the accuracy of the nomogram standardization (29). No BMD-, DXA-, or T-score-related variables were included as predictors in the LASSO procedure, logistic regression risk-score construction, or nomogram development; the risk score was derived exclusively from transcriptomic biomarkers and the nomogram incorporated the transcriptomic risk score together with non-BMD clinical variables only.

*Decision curve analysis (DCA)*. DCA is a recently developed tool for evaluating screening and diagnostic procedures (30). The present study used DCA to compare the net benefits of the risk score model. A likelihood threshold of 0.4 was selected for analysis. BMD/T-score-related variables were used only as comparator curves in the ROC and DCA analyses and were not used as model predictors or incorporated into the risk-score formula.

*Validation in a clinical cohort*

*Study design and population*. The present cross-sectional study recruited postmenopausal women from the orthopedic ward of Fourth Affiliated Hospital of School of Medicine and International School of Medicine, Zhejiang University, Zhejiang China. The inclusion criteria were: i) Postmenopausal females ≥60 years; ii) ability to undergo BMD screening; iii) ability to complete a questionnaire and provide relevant health information and iv) voluntary participation in the present study and signed an informed consent form. The exclusion criteria were: i) history of secondary OS due to an underlying disease; ii) history of drug-induced secondary osteoporosis; and iii) history of malignancy. Patients in the institutional validation cohort were recruited between April 27, 2022 and May 1, 2024. The diagnostic outcome in the present study was PMOP status. PMOP was defined according to DXA-derived BMD T-score criteria (8), with osteoporosis defined as a T-score of ≤2.5 at the lumbar spine, femoral neck, or total hip. Fragility fracture status was not used to define the diagnostic outcome and no fragility fracture-defined cases were included in either cohort.

A total of 18 whole blood samples were collected, including nine from patients with PMOP and nine from age-matched healthy controls, from The Fourth Affiliated Hospital of School of Medicine and International School of Medicine. The present study was approved by the Ethics Committee of The Fourth Affiliated Hospital of School of Medicine and International School of Medicine (approval no. K2022076; approval date April 26, 2022) and was conducted in accordance with the Declaration of Helsinki. All the participants (aged 61-79 years) provided written informed consent.

*RNA extraction and sequencing*. At The Fourth Affiliated Hospital of School of Medicine and International School of Medicine, RNA samples were collected from nine healthy controls and nine patients with PMOP for validation. Peripheral whole blood samples (20 ml) were collected from each participant between 6:00 and 8:00 during fasting and stored at -80˚C until further analysis. RNA was extracted using RNeasy columns (Qiagen GmbH) and treated with the RNase-Free DNase Set (Qiagen GmbH) after ~10 ml was collected in PAXgene Blood RNA tubes. RNA concentration and purity were assessed using the Qubit 3.0 (Thermo Fisher Scientific, Inc.), using the Qubit RNA Broad Range Assay Kit (Thermo Fisher Scientific, Inc.). Ribosomal RNA (rRNA) and globin RNA were depleted using the Ribo-Off Globin and rRNA Depletion Kit (Human/Mouse/Rat)-N408 (Vazyme Biotech Co., Ltd.), following the manufacturer's protocol. Sequencing libraries were prepared and paired-end 150 bp sequencing was performed on the Illumina NovaSeq 6000 platform (Illumina, Inc.). Gene expression levels for both mRNAs and lncRNAs were quantified as reads per kilobase per million mapped reads (RPKM) (31). For genes with multiple transcripts, the longest transcript was used for annotation and quantification, based on the GRCh38 human reference genome. To validate the predictive performance of the nomogram, gene expression data and clinical information from the validation cohort were analyzed using ROC and DCA. To harmonize the expression values across the microarray (training) and RNA sequencing (RNA-seq; validation) platforms, RPKM values from the validation cohort were $\log_2$-transformed after adding a pseudo-count of 1. Gene-level expression values were standardized to a mean of zero and unit variance using the mean and standard deviation of the corresponding genes in the microarray training dataset (gene-wise z-score standardization). Batch effects between the two platforms were corrected using ComBat from the sva R package (version 3.38.0; https://bioconductor.org/packages/sva/), with the platform type (microarray vs. RNA-seq) as the batch covariate. During validation, the same transcriptomic risk-score formula was applied to the validation cohort and no BMD-, DXA-, or T-score-related variables were entered into the validation model.

*Statistical analysis*. Pearson's $\chi^2$ test or Fisher's exact test was used to explore the differences in the distribution of clinical information. Continuous variables were compared using the t-test or Mann-Whitney U test for two groups and the Kruskal-Wallis test for multiple groups. Univariate and multivariate logistic regression analyses were performed to evaluate the impact of the risk score model along with clinical variables (age, height, weight, body mass index and smoking). All statistical analyses were conducted using R software (version 4.0; R Core Team, Vienna, Austria) and SPSS software (version 27.0; IBM Corp.). $P<0.05$ was considered to indicate a statistically significant difference. Prior to model fitting, a variance inflation factor (VIF) analysis was performed to assess collinearity among candidate predictors, including age, height, weight and body mass index (BMI). Variables with VIF ≥5 were considered indicative of significant collinearity and were removed from the final model. Based on this analysis, height and weight were excluded and only age, BMI and smoking status were retained in the final nomogram, along with the transcriptomic risk score. Complete-case analysis was used because no variables had

Table I. Clinical and biochemical features of participants in the present study.

| Characteristic | Overall | Healthy | Osteoporosis | P-value[a] |
|---|---|---|---|---|
| n | 90 | 46 | 44 | |
| Sex (Female%) | 90 (100.0) | 46 (100.0) | 44 (100.0) | NA |
| Age, years (mean SD) | 79.6 (4.1) | 78.5 (4.0) | 80.9 (3.9) | $4.000x10^{-3}$ |
| Height, cm (mean SD) | 148.5 (5.8) | 150.1 (6.0) | 146.9 (5.2) | $1.000x10^{-2}$ |
| Weight kg (mean SD) | 65.5 (12.3) | 70.1 (11.9) | 60.8 (11.0) | $<1.000x10^{-3}$ |
| BMI (mean SD) | 29.7 (5.2) | 31.2 (5.2) | 28.1 (4.8) | $5.000x10^{-3}$ |
| Neck Femur T Score (mean SD) | -2.0 (0.9) | -1.6 (0.8) | -2.5 (0.7) | $<1.000x10^{-3}$ |
| Neck Femur BMD, g/cm$^2$ (mean SD) | 0.8 (0.1) | 0.8 (0.1) | 0.7 (0.1) | $<1.000x10^{-3}$ |
| Lumbar spine T score (mean SD) | -1.7 (1.6) | -0.9 (0.7) | -3.1 (0.8) | $<1.000x10^{-3}$ |
| Lumbar Spine BMD (g/cm$^2$, mean [SD]) | 0.9 (0.2) | 1.0 (0.2) | 0.8 (0.1) | $<1.000x10^{-3}$ |
| Total hip T score (mean SD) | -1.5 (1.0) | -0.8 (0.7) | -2.0 (0.7) | $<1.000x10^{-3}$ |
| Total femur BMD, g/cm$^2$ (mean SD) | 0.8 (0.1) | 0.8 (0.1) | 0.7 (0.1) | $<1.000x10^{-3}$ |
| Ethnicity (%) | | | | $6.000x10^{-3}$ |
| White | 27 (30.0) | 9 (19.6) | 18 (40.9) | |
| Non-White | 60 (66.7) | 37 (80.4) | 23 (52.3) | |
| Asian | 3 (3.3) | 0 (0.0) | 3 (6.8) | |
| Smoking (%) | | | | $3.100x10^{-1}$ |
| No | 81 (90.0) | 43 (93.5) | 38 (86.4) | |
| Yes | 9 (10.0) | 3 (6.5) | 6 (13.6) | |
| Family history of osteoporosis (%) | | | | $9.510x10^{-1}$ |
| No | 59 (65.6) | 31 (67.4) | 28 (63.6) | |
| Yes | 14 (15.6) | 7 (15.2) | 7 (15.9) | |
| Unknown | 17 (18.9) | 8 (17.4) | 9 (20.5) | |
| Family history of fractures (%) | | | | $4.380x10^{-1}$ |
| No | 65 (72.2) | 36 (78.3) | 29 (65.9) | |
| Yes | 6 (6.7) | 2 (4.3) | 4 (9.1) | |
| Unknown | 19 (21.1) | 8 (17.4) | 11 (25.0) | |
| Calcium supplementation (%) | | | | $2.750x10^{-1}$ |
| No | 57 (63.3) | 32 (69.6) | 25 (56.8) | |
| Yes | 33 (36.7) | 14 (30.4) | 19 (43.2) | |
| Vitamin D3 Supplement (%) | | | | $9.600x10^{-2}$ |
| No | 41 (45.6) | 25 (54.3) | 16 (36.4) | |
| Yes | 49 (54.4) | 21 (45.7) | 28 (63.6) | |
| Diabetes mellitus (%) | | | | $6.700x10^{-2}$ |
| No | 63 (70.0) | 28 (60.9) | 35 (79.5) | |
| Yes | 27 (30.0) | 18 (39.1) | 9 (20.5) | |
| Dyslipidemia (%) | | | | $2.880x10^{-1}$ |
| No | 39 (43.3) | 17 (37.0) | 22 (50.0) | |
| Yes | 51 (56.7) | 29 (63.0) | 22 (50.0) | |
| Hypertension (%) | | | | $1.000x10^{0}$ |
| No | 17 (18.9) | 9 (19.6) | 8 (18.2) | |
| Yes | 73 (81.1) | 37 (80.4) | 36 (81.8) | |
| Acute myocardial infarction (%) | | | | $4.290x10^{-1}$ |
| No | 83 (92.2) | 43 (93.5) | 40 (90.9) | |
| Yes | 6 (6.7) | 2 (4.3) | 4 (9.1) | |
| Unknown | 1 (1.1) | 1 (2.2) | 0 (0.0) | |
| Creatinine, mg/dl [median (IQR)] | 0.8 [0.7, 1.0] | 0.8 [0.8, 1.0] | 0.8 [0.7, 0.9] | $9.300x10^{-2}$ |
| iPTH, pg/dl, [median (IQR)] | 57.5 [43.0, 69.0] | 58.0 [47.2, 68.5] | 54.5 [38.5, 69.2] | $4.150x10^{-1}$ |
| Alkaline phosphatase U/L [median (IQR)] | 73.0 [62.0, 94.5] | 73.0 [62.5, 96.0] | 74.0 [60.8, 92.0] | $8.310x10^{-1}$ |

Table I. Continued.

| Characteristic | Overall | Healthy | Osteoporosis | P-value[a] |
|---|---|---|---|---|
| Serum calcium, mg/dl [median (IQR)] | 9.6 [9.3, 10.0] | 9.7 [9.4, 10.1] | 9.6 [9.3, 9.8] | $2.810x10^{-1}$ |
| 25OHD, ng/ml, [median (IQR)] | 22.0 [17.0, 26.0] | 22.0 [17.2, 27.8] | 22.0 [17.0, 25.0] | $8.940x10^{-1}$ |

[a]Kolmogorov-Smirnov test was used to evaluate normal distribution. The P-values were used for comparisons of means (Student's t-test or Mann-Whitney U test) or proportions ($\chi^2$ test or Fisher's test). Statistical significance was set at P<0.05. 25OHD, 25-hydroxyvitamin D; BMD, bone mineral density; iPTH, intact parathyroid hormone.

Table II. Top 10 most upregulated and downregulated differentially expressed genes between healthy and osteoporosis group.

| Symbol | logFC | AveExpr | t | Adj P-value | B |
|---|---|---|---|---|---|
| HIST1H3H | 0.570 | 8.006 | 3.467 | $8.060x10^{-4}$ | -0.635 |
| RNA5SP85 | 0.557 | 12.495 | 3.628 | $4.720x10^{-4}$ | -0.178 |
| RNA5SP19 | 0.517 | 10.681 | 3.402 | $9.980x10^{-4}$ | -0.817 |
| SNORD70 | 0.515 | 8.462 | 2.713 | $7.985x10^{-3}$ | -2.564 |
| HIST1H4C | 0.510 | 7.992 | 3.558 | $5.960x10^{-4}$ | -0.378 |
| OTTHUMG00000150349 | 0.456 | 8.628 | 2.055 | $4.278x10^{-2}$ | -3.919 |
| RNA5SP134 | 0.445 | 10.906 | 3.935 | $1.630x10^{-4}$ | 0.735 |
| TRBV29-1 | 0.426 | 7.506 | 2.640 | $9.765x10^{-3}$ | -2.730 |
| RNA5SP86 | 0.425 | 12.437 | 3.341 | $1.216x10^{-3}$ | -0.985 |
| RNA5SP150 | 0.411 | 14.803 | 2.831 | $5.723x10^{-3}$ | -2.288 |
| SCARNA1 | -0.532 | 5.547 | -4.464 | $2.310x10^{-5}$ | 2.427 |
| RNU6ATAC | -0.651 | 5.461 | -4.658 | $1.090x10^{-5}$ | 3.079 |
| RNU5E-1 | -0.716 | 9.034 | -2.455 | $1.601x10^{-2}$ | -3.134 |
| SNORA65 | -0.794 | 7.482 | -5.982 | $4.320x10^{-8}$ | 7.896 |
| RNU5E-4P | -0.802 | 4.996 | -5.946 | $5.070x10^{-8}$ | 7.757 |
| RNU5E-2P | -0.818 | 9.693 | -3.588 | $5.400x10^{-4}$ | -0.293 |
| RNU5D-2P | -0.924 | 8.847 | -3.924 | $1.691x10^{-4}$ | 0.704 |
| SNORA53 | -0.937 | 6.523 | -5.740 | $1.250x10^{-7}$ | 6.973 |
| SNORA75 | -0.996 | 6.536 | -5.732 | $1.290x10^{-7}$ | 6.943 |
| SNORA23 | -1.432 | 11.518 | -5.174 | $1.360x10^{-6}$ | 4.887 |

AveExpr, average expression.

>5% missing data. Therefore, BMD/T-score-related variables were not entered into the multivariable model or final nomogram; they were retained only for descriptive or benchmark comparison purposes in ROC/DCA analyses.

## Results

*Baseline characteristics of the training group*. The training group comprised 90 women (46 healthy controls and 44 patients with PMOP). Smoking status, family history of OP or fractures, calcium or vitamin D3 supplementation, diabetes mellitus, dyslipidemia, hypertension and acute myocardial infarction did not differ markedly between the healthy control and PMOP groups. Bone turnover markers and biochemical indices, including creatinine, iPTH, alkaline phosphatase, serum calcium and 25-hydroxyvitamin D, were not markedly different between the groups. The participant characteristics are presented in Table I.

*Identification of DEGs*. Based on the differential expression analysis, 1,265 genes were differentially regulated, comprising 609 upregulated and 656 downregulated genes. A volcano plot of these DEGs is shown in Fig. 1. Table II lists the top 10 upregulated and downregulated DEGs selected for subsequent analyses.

*GO and Reactome analyses of DEGs*. Upregulated genes in the PMOP group were markedly enriched in BP terms related to nucleosome assembly, protein peptidyl-prolyl isomerization and DNA replication-dependent nucleosome assembly. CC terms were enriched for nucleosomes, intracellular membrane-bound organelles and nuclear nucleosomes. MF terms showed enrichment for protein heterodimerization activity and peptidyl-prolyl cis-trans isomerase activity. Reactome pathway analysis revealed significant enrichment of SRP-dependent co-translational protein targeting to membrane and mitotic prophase pathways (Table III).

Table III. GO functional annotation and Reactome pathway enrichment analysis for the upregulated DEGs.

| Category | Term ID | Term description | False discovery rate |
|---|---|---|---|
| Biological Process | GO:0006334 | Nucleosome assembly | $1.210 \times 10^{-2}$ |
| | GO:0000413 | Protein peptidyl-prolyl isomerization | $1.380 \times 10^{-2}$ |
| | GO:0006335 | DNA replication-dependent nucleosome assembly | $1.380 \times 10^{-2}$ |
| | GO:0006342 | Chromatin silencing | $1.380 \times 10^{-2}$ |
| | GO:0006613 | Cotranslational protein targeting to membrane | $1.380 \times 10^{-2}$ |
| | GO:0016458 | Gene silencing | $1.380 \times 10^{-2}$ |
| | GO:0018208 | Peptidyl-proline modification | $1.380 \times 10^{-2}$ |
| | GO:0044267 | Cellular protein metabolic process | $1.380 \times 10^{-2}$ |
| | GO:0065004 | Protein-DNA complex assembly | $1.380 \times 10^{-2}$ |
| | GO:0090150 | Establishment of protein localization to membrane | $1.380 \times 10^{-2}$ |
| Cellular Component | GO:0000786 | Nucleosome | $2.240 \times 10^{-7}$ |
| | GO:0043231 | Intracellular membrane-bounded organelle | $9.550 \times 10^{-6}$ |
| | GO:0000788 | Nuclear nucleosome | $1.900 \times 10^{-4}$ |
| | GO:0043227 | Membrane-bounded organelle | $2.300 \times 10^{-4}$ |
| | GO:0000790 | Nuclear chromatin | $1.130 \times 10^{-2}$ |
| | GO:0043229 | Intracellular organelle | $1.250 \times 10^{-2}$ |
| | GO:0000785 | Chromatin | $1.640 \times 10^{-2}$ |
| | GO:0005622 | Intracellular | $1.650 \times 10^{-2}$ |
| | GO:0005634 | Nucleus | $2.150 \times 10^{-2}$ |
| | GO:0005789 | Endoplasmic reticulum membrane | $2.150 \times 10^{-2}$ |
| Molecular Function | GO:0046982 | Protein heterodimerization activity | $4.500 \times 10^{-3}$ |
| | GO:0003755 | Peptidyl-prolyl cis-trans isomerase activity | $6.200 \times 10^{-3}$ |
| Reactome Pathway | HSA:1799339 | SRP-dependent cotranslational protein targeting to membrane | $1.610 \times 10^{-2}$ |
| | HSA:68875 | Mitotic prophase | $3.010 \times 10^{-2}$ |

GO, Gene Ontology; DEGs, differentially expressed genes.

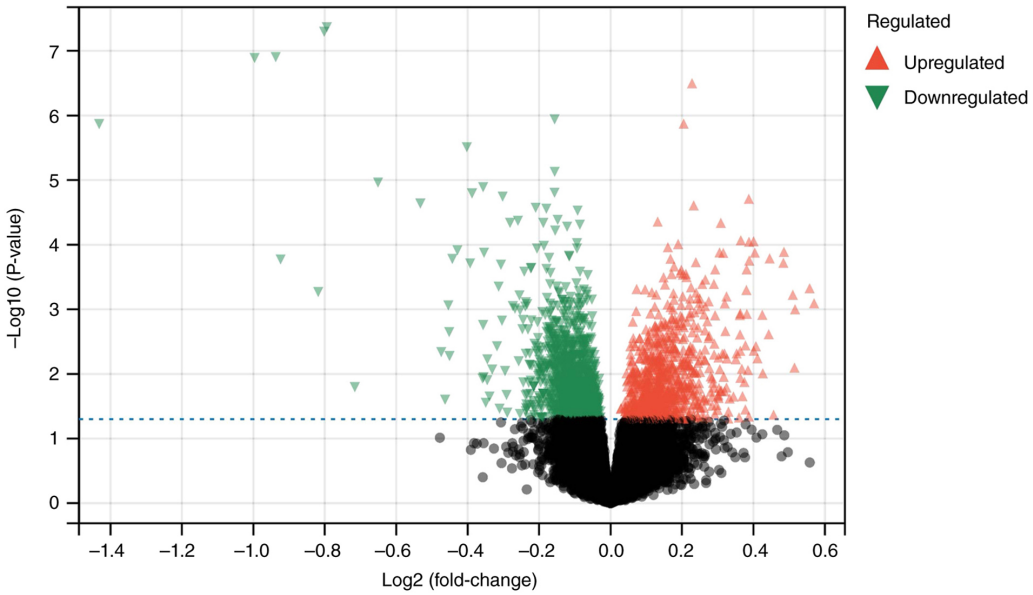


Figure 1. Volcano plot of DEGs. The black dots represent genes that are not differentially expressed, while the red and green dots, respectively, reflect upregulated and downregulated genes. DEGs, differentially expressed genes.

As shown in Table IV, downregulated genes were markedly enriched in BP terms related to stimulus detection, peptide cross-linking and G protein-coupled receptor (GPCR) signaling pathways. CC terms were enriched for the cornified

Table IV. GO functional annotation and Reactome pathway enrichment analysis for the downregulated DEGs.

| Category | Term ID | Term description | False discovery rate |
|---|---|---|---|
| Biological Process | GO:0007608 | Sensory perception of smell | $2.990 \times 10^{-8}$ |
| | GO:0050911 | Detection of chemical stimulus involved in sensory perception of smell | $2.990 \times 10^{-8}$ |
| | GO:0050906 | Detection of stimulus involved in sensory perception | $2.010 \times 10^{-7}$ |
| | GO:0051606 | Detection of stimulus | $6.960 \times 10^{-6}$ |
| | GO:0018149 | Peptide cross-linking | $3.540 \times 10^{-5}$ |
| | GO:0007600 | Sensory perception | $4.150 \times 10^{-5}$ |
| | GO:0050877 | Nervous system process | $2.300 \times 10^{-3}$ |
| | GO:0007186 | G protein-coupled receptor signaling pathway | $3.600 \times 10^{-3}$ |
| | GO:0050896 | Response to stimulus | $7.900 \times 10^{-3}$ |
| | GO:0003008 | System process | $1.090 \times 10^{-2}$ |
| Cellular Component | GO:0001533 | Cornified envelope | $6.270 \times 10^{-5}$ |
| | GO:0005886 | Plasma membrane | $1.450 \times 10^{-2}$ |
| | GO:0005623 | Cell | $3.250 \times 10^{-2}$ |
| | GO:0005811 | Lipid droplet | $3.250 \times 10^{-2}$ |
| Molecular Function | GO:0004984 | Olfactory receptor activity | $6.870 \times 10^{-9}$ |
| | GO:0004888 | Transmembrane signaling receptor activity | $1.200 \times 10^{-4}$ |
| | GO:0060089 | Molecular transducer activity | $1.400 \times 10^{-4}$ |
| | GO:0004930 | G protein-coupled receptor activity | $2.700 \times 10^{-4}$ |
| | GO:0038023 | Signaling receptor activity | $2.700 \times 10^{-4}$ |
| | GO:0036459 | Thiol-dependent ubiquitinyl hydrolase activity | $2.100 \times 10^{-3}$ |
| | GO:0030332 | Cyclin binding | $4.470 \times 10^{-2}$ |
| | GO:1990380 | Lys48-specific deubiquitinase activity | $4.470 \times 10^{-2}$ |
| Reactome pathway | HSA:381753 | Olfactory signaling pathway | $9.210 \times 10^{-9}$ |
| | HSA:418555 | G alpha (s) signaling events | $1.900 \times 10^{-8}$ |
| | HSA:162582 | Signal transduction | $3.400 \times 10^{-4}$ |
| | HSA:372790 | Signaling by GPCR | $1.900 \times 10^{-3}$ |
| | HSA:388396 | GPCR downstream signaling | $3.700 \times 10^{-3}$ |
| | HSA:6809371 | Formation of the cornified envelope | $1.690 \times 10^{-2}$ |
| | HSA:1855167 | Synthesis of pyrophosphates in the cytosol | $3.140 \times 10^{-2}$ |
| | HSA:264870 | Caspase-mediated cleavage of cytoskeletal proteins | $4.300 \times 10^{-2}$ |

GO, Gene Ontology; DEGs, differentially expressed genes.

envelope, plasma membrane and cellular structures, whereas MF terms were enriched for transmembrane signaling receptor activity, GPCR activity and cyclin binding. Reactome pathway analysis identified significant enrichment in G alpha (s) signaling events, signal transduction and GPCR downstream signaling pathways.

*PPI network construction and hub gene identification*. STRING techniques were used to predict the connections between the DEGs. The PPI network (PPI enrichment, P<1.78e-15) of the upregulated DEGs included 258 nodes and 430 edges (Fig. S1). The top 30 upregulated genes are shown in Fig. 2A and Table V. The PPI network (PPI enrichment, P<1.53e-09) of the DEGs included 228 nodes and 225 edges (Fig. S2) and the top 30 downregulated genes are shown in Fig. 2B and Table V. GAPDH, HIST1H2AC, HIST1H2BM, HIST1H2AA,HIST1H4C,HIST1H4J,UBE2D3,HIST1H2AH, HIST3H3 and RPL35 were among the top 10 upregulated hub genes. Meanwhile, ADRBK1, NOTCH1, SPRR1A, SPRR3, SPRR2D, LCE1E, SPRR2F, LCE1D, S100A7 and EIF4G1 were among the top 10 downregulated hub genes. The upregulated gene comprised the 10 upregulated hub genes, whereas the downregulated set comprised the 10 downregulated hub genes.

*GSEA*. GSEA indicated significant enrichment of the IL6/JAK/STAT3 signaling pathway in the PMOP group [normalized enrichment score (NES)=0.90, size=65], whereas the estrogen response pathway was markedly enriched in the control group in both the early (NES=-1.32, size=131) and late (NES=-1.39, size=129) stages (Fig. 3).

*Screening of risk genes*. LASSO logistic regression was used to develop an optimized predictive model. Signal genes from GSEA (such as IL6/JAK/STAT3 and estrogen response pathways) and dysregulated genes (including upregulated

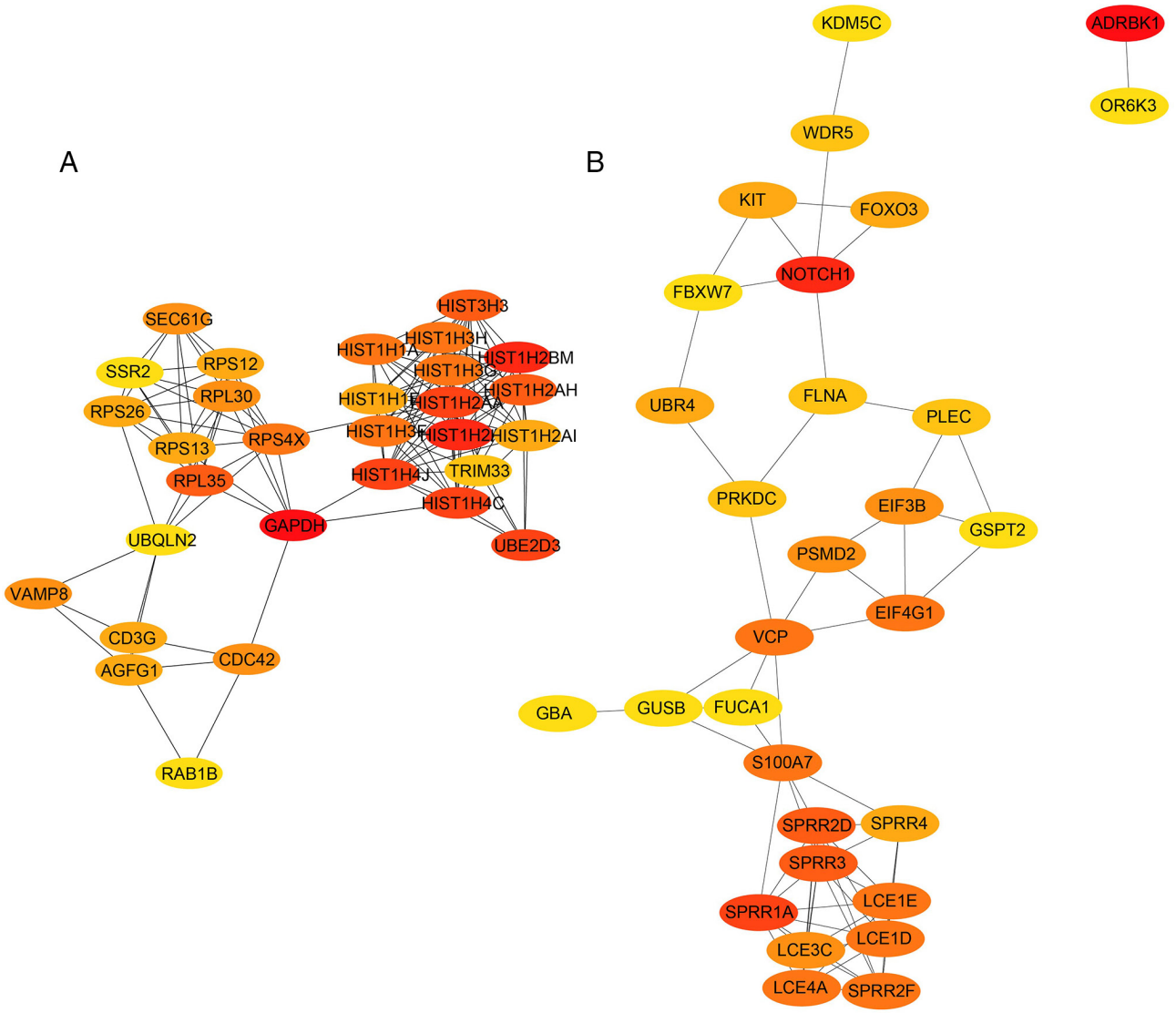


Figure 2. Hub-gene identification in upregulated and downregulated DEGs. (A) The top 30 hub genes of the significant upregulated DEGs. (B) The top 30 hub genes of the significant downregulated DEGs. DEGs, differentially expressed genes.

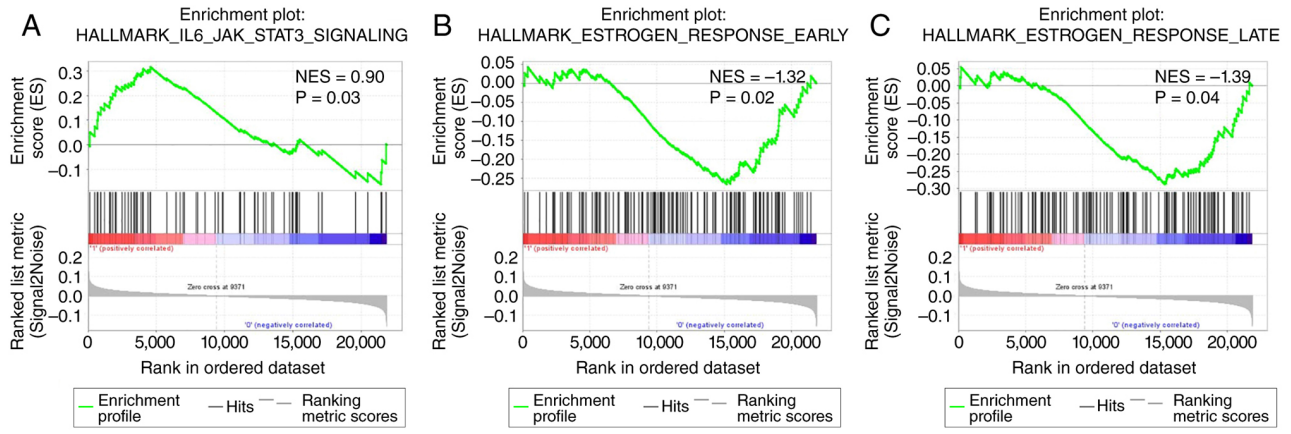


Figure 3. GSEA analysis indicated that IL6 JAK STAT3 signaling was markedly enriched in the OP group (A) while estrogen response early (B) and late (C) were markedly enriched in the healthy group. GSEA, Gene Set Enrichment Analysis; OP, osteoporosis; NES, normalized enrichment score.

and downregulated genes) were selected for further analysis (Fig. 4).

*ROC curves and nomogram*. The omnibus test validated the model coefficients, indicating that models based on

Table V. Top 30 hub genes in protein-protein interaction network.

| Upregulated gene | Degree of connectivity | Downregulated gene | Degree of connectivity |
|---|---|---|---|
| GAPDH | 24 | ADRBK1 | 28 |
| HIST1H2AC | 17 | NOTCH1 | 11 |
| HIST1H2BM | 17 | SPRR1A | 10 |
| HIST1H2AA | 16 | SPRR3 | 9 |
| HIST1H4C | 16 | SPRR2D | 9 |
| HIST1H4J | 16 | LCE1E | 8 |
| UBE2D3 | 16 | SPRR2F | 8 |
| HIST1H2AH | 15 | LCE1D | 8 |
| HIST3H3 | 15 | S100A7 | 8 |
| RPL35 | 15 | EIF4G1 | 8 |
| HIST1H3G | 14 | LCE4A | 8 |
| HIST1H3F | 14 | VCP | 8 |
| HIST1H3H | 14 | LCE3C | 7 |
| RPS4X | 14 | PSMD2 | 7 |
| HIST1H1A | 14 | EIF3B | 7 |
| SEC61G | 13 | SPRR4 | 6 |
| RPL30 | 13 | FOXO3 | 6 |
| CDC42 | 13 | KIT | 6 |
| VAMP8 | 13 | UBR4 | 6 |
| HIST1H1E | 12 | PRKDC | 5 |
| HIST1H2AI | 12 | FLNA | 5 |
| RPS12 | 12 | PLEC | 5 |
| RPS13 | 12 | WDR5 | 5 |
| RPS26 | 12 | USP17L19 | 4 |
| AGFG1 | 12 | USP17L21 | 4 |
| CD3G | 12 | USP17L18 | 4 |
| TRIM33 | 11 | USP17L15 | 4 |
| SSR2 | 10 | USP17L12 | 4 |
| SSR1 | 10 | GBA | 4 |
| FYB | 10 | GUSB | 4 |

downregulated genes group (P=0.002) and estrogen response genes (P<0.001) were significant, whereas models based on upregulated genes group (P=0.053) and IL6/JAK/STAT3 signaling (P=0.318) were not. The ROC curves analysis revealed that the area under the curve (AUC) for the lumbar spine T-score model was the highest (AUC=0.905), whereas that AUC for downregulated genes was the lowest (AUC=0.533; Fig. 5).

Based on these results, 13 genes from the estrogen group were selected to construct a risk score model. The detailed formula was: Risk score=(-5.324 x CD44) + (-1.101 x FDFT1) + (-1.081 x SLC29A1) + (-0.24 x P2RY2) + (-0.55 x RHOBTB3) + (-3.204 x TNNC1) + (-1.135 x RPS6KA2) + (-6.317 x TSKU) + (-5.31 x CYP26B1) + (-16.837 x SEMA3B) + (-5.126 x SYT12) + (-2.226 x IL17RB) + (-4.814 x ELF3) + 298.473. This model achieved an AUC value of 0.880 (Fig. 6A). A nomogram integrating clinical variables and risk scores demonstrated strong predictive power (Fig. 6B). Among the 90 individuals studied, the nomogram calibration curve for predicting PMOP showed promising results (Fig. 6C).

*Risk score as an independent risk predictor of PMOP.* Univariate and multivariate logistic regression analyses confirmed that the risk score was an independent risk factor for PMOP (Fig. 7).

*DCA.* The decision curves for the five predictive models for PMOP in the testing datasets are shown in Fig. 8. Among the predictive models, the total hip T-score demonstrated the lowest net benefit, indicating limited predictive value. By contrast, the model integrating the risk score with clinical variables exhibited the highest net benefit, suggesting a superior predictive performance.

*Validation of risk score model.* The validation cohort included 18 women (nine healthy and nine with PMOP). No significant differences were observed between the two groups (healthy vs. PMOP) in terms of smoking, family history of OP, fractures, calcium and vitamin D3 supplementation, diabetes mellitus, dyslipidemia, hypertension and acute myocardial infarction. Bone turnover markers and biochemical indices, including creatinine, iPTH, alkaline phosphatase, serum calcium and 25-hydroxyvitamin D levels, were not markedly different between the groups. Detailed characteristics of the participants are summarized in Table VI.

Differential expression analysis identified 823 differentially expressed genes (DEGs) comprising 506 upregulated and 317 downregulated genes. Volcano plots illustrating DEGs are shown in Fig. 9A. Expression data from the validation group were normalized and used to evaluate the performance of the risk score model. The same formula was applied to calculate individual risk scores and the ROC curve analysis demonstrated that the model effectively distinguished PMOP from controls, yielding an AUC of 0.790 (Fig. 9B).

## Discussion

Early identification of PMOP before significant BMD reduction holds substantial clinical value, enabling timely patient selection and early intervention (32). The present study developed a clinical prediction nomogram that integrates transcriptomic data with clinical variables from a training cohort. The model was validated using high-throughput RNA sequencing data and clinical information from an independent cohort. The nomogram showed promising preliminary predictive performance and potential clinical applicability for early PMOP diagnosis.

To construct the risk score model, the present study analyzed PMOP-associated transcriptomic data from the GEO database and identified 1,265 DEGs, including 609 upregulated and 656 downregulated genes. These genes were involved in BP and pathways such as nucleosome assembly, protein peptidyl-prolyl isomerization, DNA replication-dependent nucleosome assembly, SRP-dependent cotranslational protein targeting to the membrane, G protein-coupled receptor signaling pathway and GPCR downstream signaling. Previous studies have identified key molecules in osteogenic differentiation, including peptidyl-prolyl isomerase 1 (Pin1), which interacts with Osterix to modulate protein stability and transcriptional activity (33,34). Additionally, G protein-coupled receptor 35 (GPR35) has been implicated in osteogenesis via

Table VI. Clinical and biochemical features of participants in the validation group of the present study.

| Characteristic | Overall | Healthy | Osteoporosis | P-value[a] |
|---|---|---|---|---|
| n | 18 | 9 | 9 | |
| Sex (Female%) | 18 (100.0) | 9 (100.0) | 9 (100.0) | NA |
| Age, years, mean (SD) | 71.0 (4.4) | 72.1 (2.9) | 69.9 (5.7) | $3.100x10^{-1}$ |
| Height, cm, mean (SD) | 155.6 (6.4) | 158.9 (5.7) | 152.3(5.6) | $3.000x10^{-2}$ |
| Weight, kg, mean (SD) | 57.8 (12.0) | 65.9 (8.7) | 49.7 (9.2) | $1.400x10^{-3}$ |
| BMI, mean (SD) | 23.7 (4.1) | 26.0 (2.5) | 21.5 (4.2) | $2.000x10^{-2}$ |
| Neck femur T score, mean (SD) | -1.4 (1.0) | -0.7 (0.7) | -2.1 (0.7) | $<1.000x10^{-3}$ |
| Neck Femur BMD, g/cm$^2$, mean (SD) | 0.8 (0.1) | 0.7 (0.1) | 0.6 (0.1) | $<1.000x10^{-3}$ |
| Lumbar spine T score, mean (SD) | -2.0 (1.3) | -0.7 (1.4) | -2.7 (1.1) | $<1.000x10^{-3}$ |
| Lumbar spine BMD, g/cm$^2$, mean (SD) | 0.9 (0.2) | 1.0 (0.1) | 0.7 (0.1) | $<1.000x10^{-3}$ |
| Total hip T score, mean (SD) | -1.6 (1.1) | -0.8 (0.7) | -2.5 (0.7) | $<1.000x10^{-3}$ |
| Total femur BMD, g/cm$^2$ (mean SD) | 0.8 (0.1) | 0.9 (0.1) | 0.7 (0.1) | $<1.000x10^{-3}$ |
| Ethnicity, n (%) | | | | |
| White | 0 (0) | 0 (0) | 0 (0) | NA |
| Non-White | 18 (100.0) | 9 (100.0) | 9 (100.0) | NA |
| Asian | 18 (100.0) | 9 (100.0) | 9 (100.0) | NA |
| Smoking, n (%) | 0 (0) | 0 (0) | 0 (0) | NA |
| No | 18 (100.0) | 9 (100.0) | 9 (100.0) | NA |
| Yes | 0 (0) | 0 (0) | 0 (0) | NA |
| Family history of osteoporosis, n (%) | | | | $6.200x10^{-1}$ |
| No | 6 (33.3) | 3 (33.3) | 3 (33.3) | |
| Yes | 4 (22.2) | 1 (11.1) | 3 (33.3) | |
| Unknown | 8 (44.4) | 5 (55.5) | 3 (33.3) | |
| Family history of fractures, n (%) | | | | $8.130x10^{-1}$ |
| No | 10 (61.1) | 6 (66.7) | 4 (55.6) | |
| Yes | 4 (11.1) | 1 (11.1) | 3 (11.1) | |
| Unknown | 5 (27.8) | 2 (22.2) | 2 (33.3) | |
| Calcium supplementation, n (%) | | | | $3.100x10^{-1}$ |
| No | 12 (66.7) | 5 (55.6) | 7 (77.8) | |
| Yes | 6 (33.3) | 4 (44.4) | 2 (22.2) | |
| Vitamin D3 supplement, n (%) | | | | $1.670x10^{-1}$ |
| No | 11 (61.1) | 4 (44.4) | 7 (77.8) | |
| Yes | 7 (38.9) | 5 (55.6) | 2 (22.2) | |
| Diabetes mellitus, n (%) | | | | $2.880x10^{-1}$ |
| No | 14 (77.8) | 6 (66.7) | 8 (88.9) | |
| Yes | 4 (22.2) | 3 (33.3) | 1 (11.1) | |
| Dyslipidemia, n (%) | | | | $3.190x10^{-1}$ |
| No | 10 (55.6) | 6 (66.7) | 4 (44.4) | |
| Yes | 8 (44.4) | 3 (33.3) | 5 (55.6) | |
| Hypertension, n (%) | | | | $1.730x10^{-1}$ |
| No | 9 (50.0) | 3 (33.3) | 6 (66.7) | |
| Yes | 9 (50.0) | 6 (66.7) | 3 (33.3) | |
| Acute myocardial infarction, n (%) | | | | NA |
| No | 18 (100.0) | 9 (100.0) | 9 (100.0) | |
| Yes | 0 (0) | 0 (0) | 0 (0) | |
| Creatinine, mg/dl, median [IQR] | 0.6 [0.5, 0.7] | 0.6 [0.5, 0.6] | 0.6 [0.6, 0.7] | $5.690x10^{-1}$ |
| iPTH, pg/dl, median [IQR] | 33.6 [26.4, 42.0] | 34.2 [27.4, 42.4] | 33.0 [26.1, 40.7] | $8.030x10^{-1}$ |
| Alkaline phosphatase U/l, median [IQR] | 86.1 [70.7, 107.3] | 80.0 [70.0, 90.0] | 92.2 [82.0, 112.0] | $2.600x10^{-1}$ |

Table VI. Continued.

| Characteristic | Overall | Healthy | Osteoporosis | P-value[a] |
|---|---|---|---|---|
| Serum calcium, mg/dl, median IQR] | 9.0 [8.7, 9.2] | 9.1 [9.1, 9.2] | 8.9 [8.6, 8.9] | $5.640x10^{-1}$ |
| 25OHD, ng/ml, median [IQR] | 23.0 [17.0, 28.6] | 23.3 [22.1, 26.6] | 22.8 [15.4, 30.0] | $8.990x10^{-1}$ |

[a]Kolmogorov-Smirnov test was used to evaluate normal distribution. The P-values were used for comparisons of means (Student's t-test or Mann-Whitney U test) or proportions ($\chi^2$ test or Fisher's test). Statistical significance was set at P<0.05. 25OHD, 25-hydroxyvitamin D; BMD, bone mineral density; iPTH, intact parathyroid hormone.

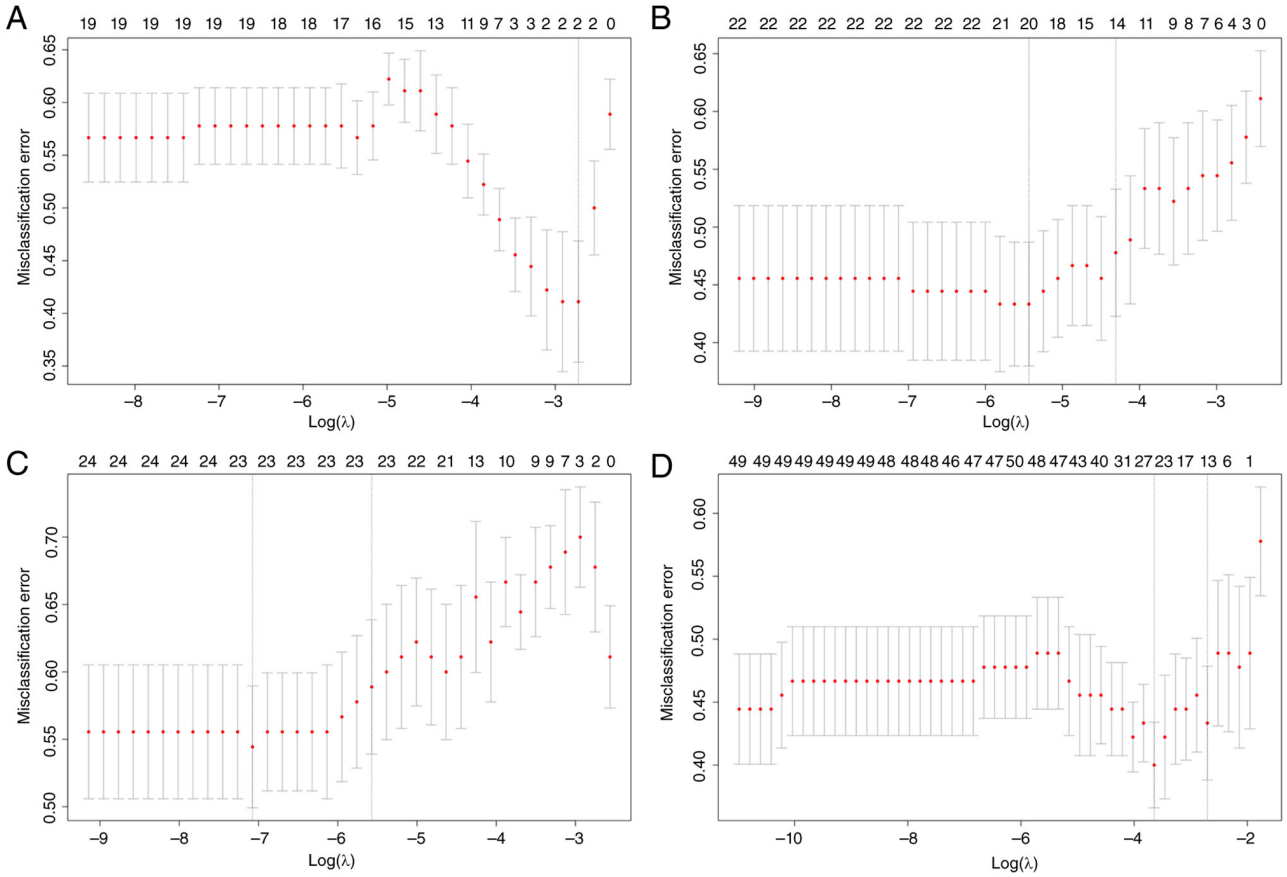


Figure 4. Misclassification error vs. log (λ) was plotted in the (A) upregulated genes group, (B) downregulated genes group, (C) IL6 JAK STAT3 signaling genes group, and (D) estrogen response genes group using the LASSO logistic regression model. LASSO, least absolute shrinkage and selection operator.

the Wnt/GSK3/β-catenin signaling pathway (35,36), whereas G-protein-coupled receptor kinase 2-interacting protein-1 (GIT1) regulates angiogenic factor secretion in bone marrow mesenchymal stem cells through NF-κB/Notch signaling to promote angiogenesis (37,38). These findings suggested that the DEGs identified in the present study may be involved in PMOP pathogenesis.

PPI network analysis was performed using STRING database to evaluate functional interactions among DEGs. The top 10 upregulated and downregulated DEGs potentially involved in PMOP pathogenesis were selected for further investigation. Downregulation of FTX via the Notch1 signaling pathway has been shown to enhance osteoclast differentiation by targeting miR-137 (39). A previous study has proposed UBE2D3 and exosomal miRNAs as potential biomarkers for predicting OS risk in postmenopausal women (40). GSEA revealed significant pathway differences between the PMOP and control groups, including estrogen response signaling and IL6/JAK/STAT3 signaling, both of which have been implicated in osteogenesis (41). Estrogen signaling is well established as a key regulator of PMOP development (42). Moreover, activation of the JAK2/STAT3 pathway has been linked to PMOP progression and its role in bone metabolism, including osteogenesis and neovascularization, has been widely reported (43,44).

Signal genes identified by GSEA (IL6/JAK/STAT3 signaling and estrogen response genes) and dysregulated genes (upregulated and downregulated genes) were selected using LASSO logistic regression to identify the most relevant predictive features with the fewest independent variables. Among the evaluated models, a 13-gene risk score model was

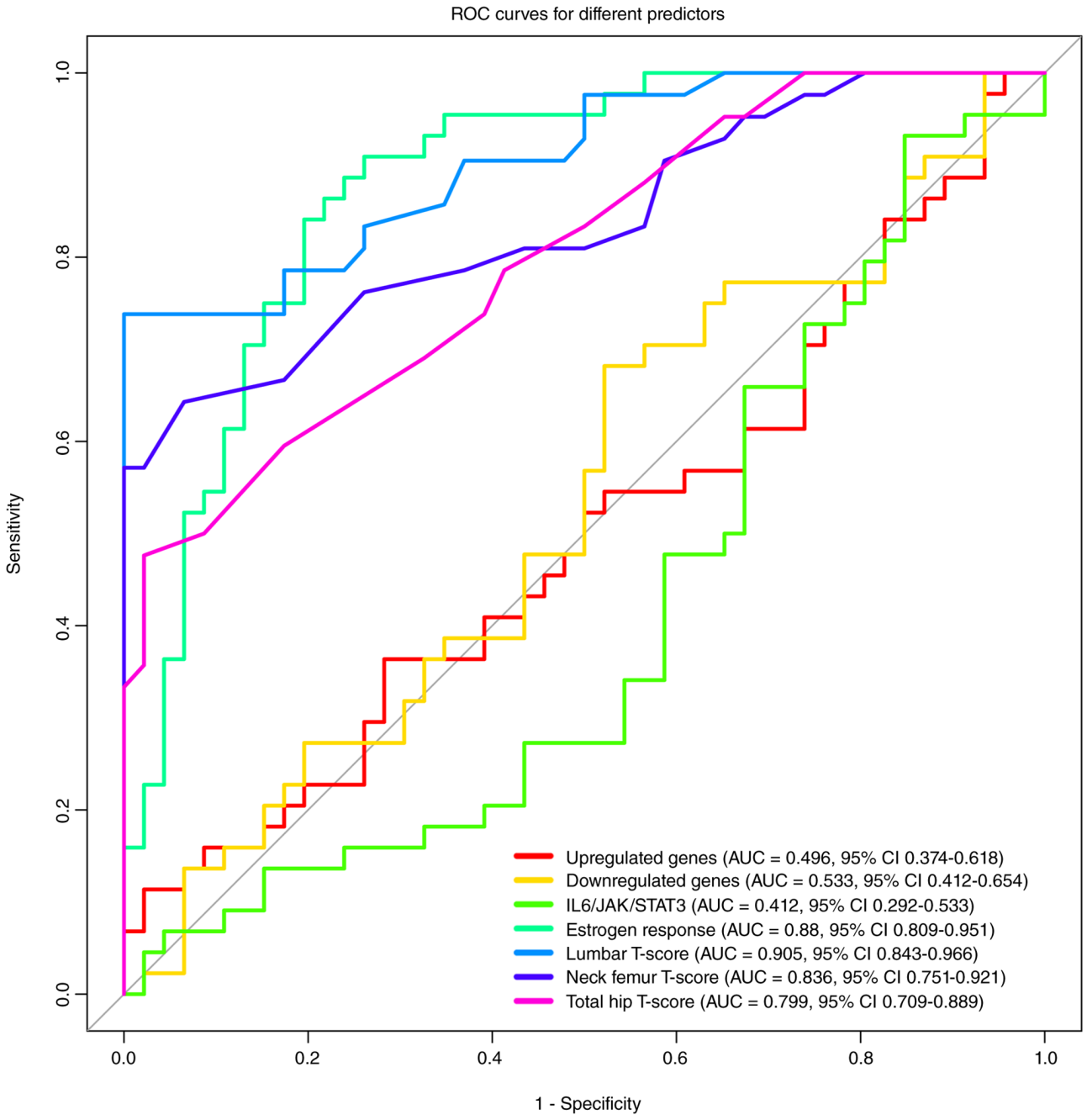


Figure 5. ROC curves of different groups. ROC, receiver operating characteristic; AUC, area under the curve; CI, confidence interval.

selected based on its superior AUC performance. The final model included CD44, FDFT1, SLC29A1, P2RY2, RHOBTB3, TNNC1, RPS6KA2, TSKU, CYP26B1, SEMA3B, SYT12, IL17RB and ELF3. Several of these genes have been associated with osteoporosis and bone metabolism. A previous bioinformatic analysis reported that CD44 was a differentially expressed Th17 cell-related hub genes (DETh17RGs) in osteoporosis and validated the hub DETh17RGs *in vivo* using quantitative PCR (45). Although CD44 is abundantly expressed on osteoblast surfaces, nanoparticles may target osteoclasts by binding to CD44 on the osteoclast surface (46). FDFT1 polymorphisms have been identified as genetic markers of osteoporosis risk in postmenopausal women (47). The osteocyte response to dynamic loading is important for regulating bone mass. Under mechanical loading, P2Y2 activation initiates a negative feedback loop that modulates the osteocyte response to continuous strain by facilitating actin stress fiber formation, thereby limiting the response to sustained mechanical stimulation (48). TNNC1 is associated with bone calcium transport and skeletal muscle movement, suggesting a potential role in bone homeostasis (49). Cyp26b1, a key enzyme in all-trans retinoic acid degradation, has emerged as a potential therapeutic target for bone-related disorders and bone tissue engineering (50). Under hyperglycemic conditions, Sema3B enhances the proliferation and osteogenic differentiation of bone marrow mesenchymal stem cells (BMSCs), suggesting involvement in bone remodeling (51). Adipogenic differentiation represents a crucial

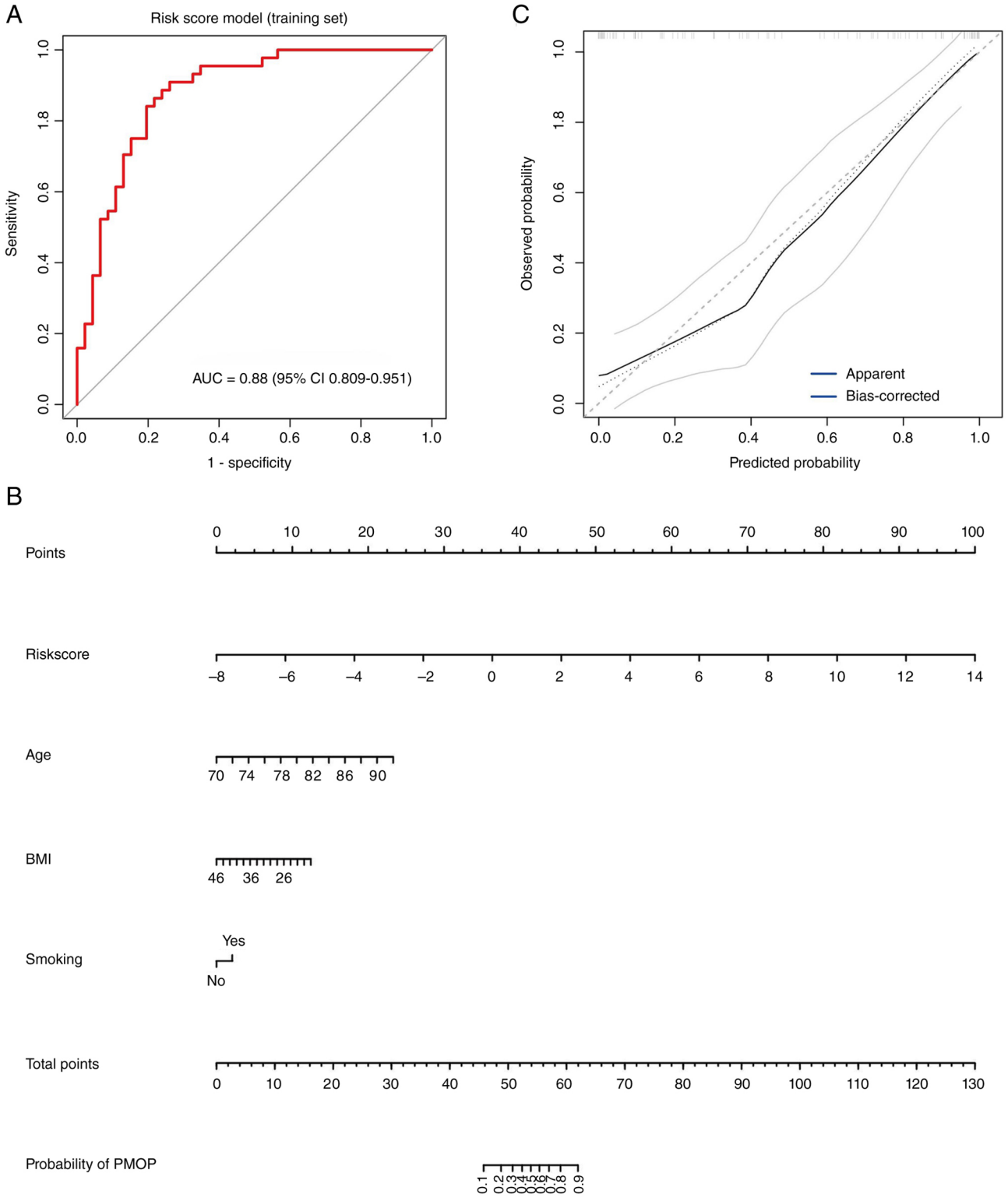


Figure 6. Diagnostic performance and nomogram construction for the estrogen-response risk score model. (A) ROC curves of the risk score model based on 13 genes from the estrogen response group. (B) Nomogram to predict OP. (C) The calibration curves of the nomogram. The anticipated predicted probability of OP is on the x-axis, whereas the actual chance is on the y-axis. A perfect prediction model is shown by the diagonal line. The solid line corresponds to the nomogram's actual performance. The tool improves at forecasting recurrence as the solid line goes closer to the diagonal one. ROC, receiver operating characteristic; OP, osteoporosis.

pathway within the lineage potential of mesenchymal stem cells (MSCs) and is relevant to OS management. E74-like factor 3 (Elf3) has been identified and validated as a pivotal hub gene governing adipogenesis in MSCs (52). Collectively, most genes in the risk score model have previously been linked to osteogenesis or OS, supporting their potential relevance to PMOP pathophysiology.

OS is a multifactorial disorder characterized by strong genetic components. Several recent studies have proposed gene signatures for PMOP risk assessment. Hu *et al* (53)

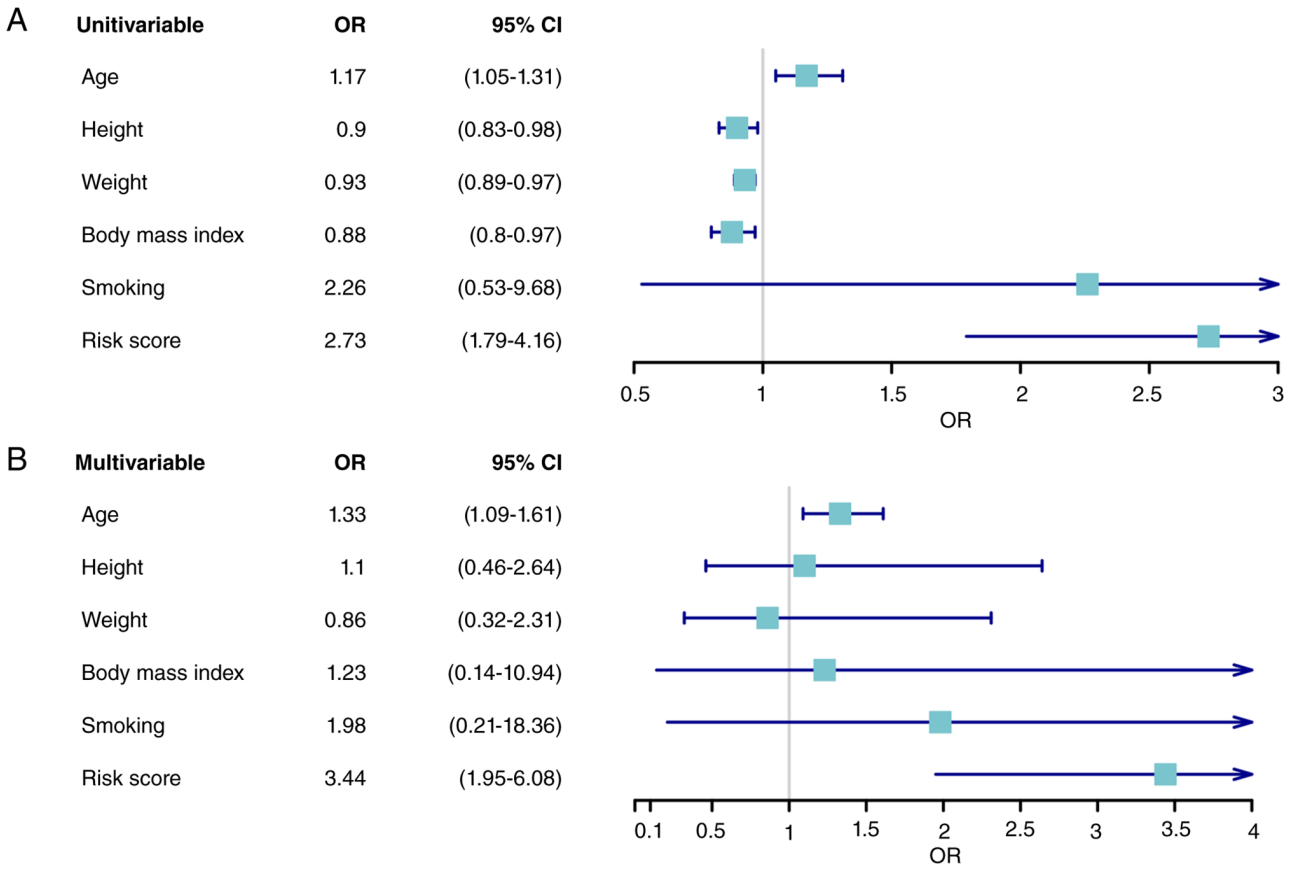


Figure 7. Logistic regression analysis of the association between the risk score model and clinical factors. (A) Univariate and (B) multivariate logistic regression analyses for evaluating the association between the risk score model and clinical factors. OR, odds ratio; CI, confidence interval.

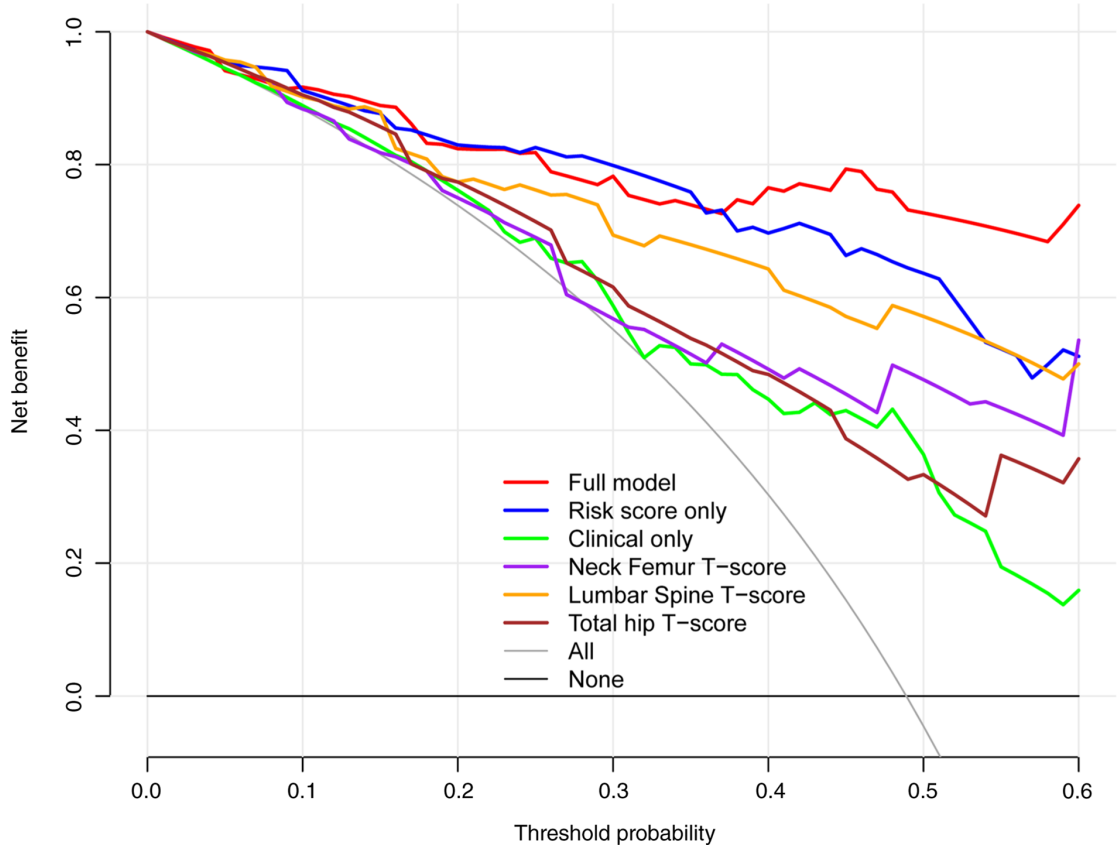


Figure 8. DCA curves of different models. DCA, decision curve analysis.

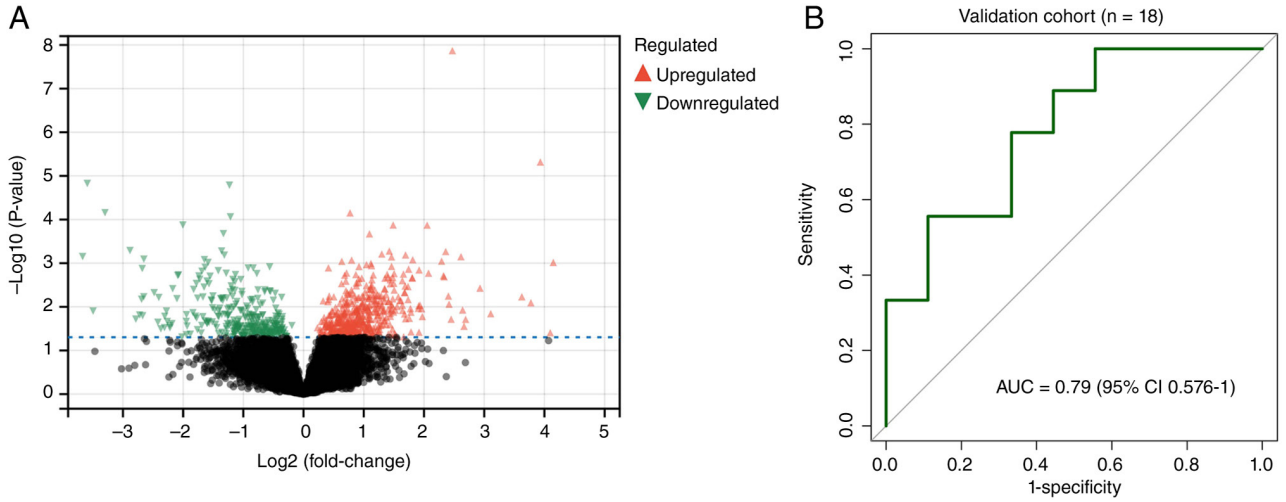


Figure 9. Validation of differential expression and risk-score model performance in the institutional cohort. (A) Volcano plot of the DEGs. The black dots represent genes that are not differentially expressed, while the red and green dots, respectively, reflect upregulated and downregulated genes. (B) ROC curves demonstrated that the risk score model performed well in The Fourth Affiliated Hospital of the Zhenjiang University School of Medicine. DEGs, differentially expressed genes; ROC, receiver operating characteristic.

developed a ferroptosis-associated gene signature for early PMOP diagnosis, whereas Gao *et al* (54) integrated 11 transcriptomic signatures and clinical examination results to formulate a risk model for improving PMOP prediction. Geng *et al* (55) constructed a PMOP-related gene signature based on SCUBE3, TNNC1, SPON1, SEPT12 and ULBP1 that may contribute to the development of preventive strategies for PMOP. Zeng *et al* (56) established a 15-gene diagnostic signature and demonstrated its effectiveness for predicting PMOP risk. Yuan *et al* (15) further clarified the roles of RAB2A and FYCO1 in PMOP pathogenesis and validated the corresponding gene signatures. Unlike these gene-only models, Wang *et al* (16) developed a clinical nomogram incorporating demographic factors such as sex, education level and body weight, which showed improved clinical benefit for PMOP screening. However, most previous models were based mainly on bioinformatic analyses with limited sequencing data and few studies have systematically evaluated the relationship between clinical variables and gene expression. The present study addressed this gap by integrating genetic and clinical factors to support clinical decision-making.

Although genetic factors play a central role in osteoporosis pathogenesis, osteoporosis is also influenced by a complex interplay of genetic, intrinsic, exogenous and lifestyle factors (57,58). To assess the predictive performance of the 13-gene risk score model, the present study first analyzed ROC curves. Univariate and multivariate logistic regression analyses were then performed to evaluate the risk score model and clinical factors. The risk score yielded an odds ratio (OR) of 2.73 [95% confidence interval (CI): 1.79-4.16] in univariate analysis and 3.44 (95% CI: 1.95-6.08) in multivariate analysis. These values were higher than those observed for traditional clinical risk factors, such as age, smoking status and BMI.

Given that OS reflects combined genetic, metabolic and environmental influences, we constructed a clinical prediction nomogram incorporating transcriptomic data (risk score model) and key clinical variables (age, smoking status and BMI). The selection of these clinical predictors is consistent with previous studies reinforcing the consensus that these factors are independent risk factors for OS (59-63). Unlike previously proposed predictive gene signatures, the nomogram of the present study integrated genetic and clinical factors and may provide a more comprehensive OS risk assessment (15,53-56,64). Moreover, DCA indicated that combining the risk score with clinical variables provided substantial clinical benefit. The nomogram was designed as a readily accessible predictive tool and is available at https://spinelhm.shinyapps.io/DynNomapp/.

The present study externally validated the predictive accuracy and clinical utility of the model using high-throughput RNA sequencing data and corresponding clinical variables from our hospital cohort. The nomogram showed promising predictive performance, with an AUC of 0.790.

Several limitations should be acknowledged. First, the training cohort (n=90) and, in particular, the external validation cohort (n=18) were small, limiting statistical power and model generalizability. The validation AUC of 0.790 has wide CIs and should be interpreted cautiously. Second, the cross-sectional design indicates that the nomogram reflects associations between predictors and OP status at a single time point and does not capture longitudinal risk or disease progression. Prospective cohort studies are needed to evaluate whether the model predicts incident OS. Third, the training and validation datasets were generated on different platforms (Affymetrix microarray vs. Illumina RNA-seq). Although ComBat batch correction and gene-wise z-score standardization were applied, residual platform-specific effects cannot be excluded. Fourth, the biological interpretation of the 13 candidate genes is based on *in silico* functional annotation and published literature; experimental validation at the mRNA and protein levels was not performed and is needed to confirm the functional relevance of these candidate biomarkers. Fifth, important clinical variables that may influence PMOP risk, including years since menopause, hormone therapy, anti-osteoporosis treatment, glucocorticoid exposure, physical activity, dietary calcium and vitamin

D intake, renal function and fracture history, were unavailable in the source dataset and could not be incorporated into the model. Finally, T-score, a component of the reference standard used to define OP, was used as a comparator in the ROC and DCA analyses. Although T-score was not used as a predictor in model construction, its use as a comparator introduces potential diagnostic circularity; therefore, ROC/DCA comparisons should be regarded as orienting benchmarks rather than formal diagnostic comparisons. Given these limitations, the nomogram should be considered an exploratory research tool. Independent external validation in larger, multicenter, prospective cohorts with comprehensive clinical phenotyping is required before clinical application.

In conclusion, the present study successfully developed a risk-score model for predicting PMOP that demonstrated strong diagnostic performance. Furthermore, based on the DCA, the integration of the risk score model and clinical factors to construct a nomogram that maximizes the net clinical benefit was recommend. The resulting clinical prediction nomogram was effective and easily accessible. However, the primary goal of this model was to predict PMOP before significant deterioration in BMD occurs. Although our findings are promising, further refinement and validation are warranted. Future studies should focus on optimizing this model to enhance its predictive accuracy and clinical applicability.

**Acknowledgements**

Not applicable.

**Funding**

The present study was supported by the Zhejiang Natural Science Foundation (grant no. LTGY24H060002) and the Central Zhejiang Science and Technology Innovation Corridor Joint Fund of the Zhejiang Provincial Natural Science Foundation of China (grant no. LJHSQY26H060003).

**Availability of data and materials**

The data generated in the present study may be requested from the corresponding author.

**Authors' contributions**

LYH, YC and LRS contributed to study design, data analysis and manuscript drafting. ZLZ, KA and HML contributed to study design and conducted the initial data interpretation. QFH and HHH contributed to study design, critical review and manuscript revision. All authors reviewed the manuscript critically. QFH and HHH confirm the authenticity of all the raw data. All authors read and approved the final version of the manuscript.

**Ethics approval and consent to participate**

The present study was approved by the Ethics Committee of The Fourth Affiliated Hospital of the Zhejiang University School of Medicine (approval no. K2022076) and was conducted in accordance with the Declaration of Helsinki. All the participants (aged 61-79 years) provided written informed consent.

**Patient consent for publication**

Not applicable.

**Competing interests**

The authors declare that they have no competing interests.

**References**

1. NIH Consensus Development Panel on Osteoporosis Prevention, Diagnosis, and Therapy, March 7-29, 2000: Highlights of the conference. South Med J 94: 569-573, 2001.
2. Si L, Winzenberg TM, Jiang Q, Chen M and Palmer AJ: Projection of osteoporosis-related fractures and costs in China: 2010-2050. Osteoporos Int 26: 1929-1937, 2015.
3. Kanis JA, Norton N, Harvey NC, Jacobson T, Johansson H, Lorentzon M, McCloskey EV, Willers C and Borgström F: SCOPE 2021: A new scorecard for osteoporosis in Europe. Arch Osteoporos 16: 82, 2021.
4. Subarajan P, Arceo-Mendoza RM and Camacho PM: Postmenopausal osteoporosis: A review of latest guidelines. Endocrinol Metab Clin North Am 53: 497-512, 2024.
5. Management of osteoporosis in postmenopausal women: The 2021 position statement of The North American Menopause Society. Menopause 28: 973-997, 2021.
6. Cheng X, Zhao K, Zha X, Du X, Li Y, Chen S, Wu Y, Li S, Lu Y, Zhang Y, *et al*: Opportunistic screening using low-dose CT and the prevalence of osteoporosis in China: A nationwide, multicenter study. J Bone Miner Res 36: 427-435, 2021.
7. Kanis JA: Diagnosis of osteoporosis and assessment of fracture risk. Lancet 359: 1929-1936, 2002.
8. LeBoff MS, Greenspan SL, Insogna KL, Lewiecki EM, Saag KG, Singer AJ and Siris ES: The clinician's guide to prevention and treatment of osteoporosis. Osteoporos Int 33: 2049-2102, 2022.
9. Slart RHJA, Punda M, Ali DS, Bazzocchi A, Bock O, Camacho P, Carey JJ, Colquhoun A, Compston J, Engelke K, *et al*: Updated practice guideline for dual-energy X-ray absorptiometry (DXA). Eur J Nucl Med Mol Imaging 52: 539-563, 2025.
10. Xian W, Xu X, Li J, Sun J, Fu H, Wu S and Liu H: Health care inequality under different medical insurance schemes in a socioeconomically underdeveloped region of China: A propensity score matching analysis. BMC Public Health 19: 1373, 2019.
11. Chew CK and Clarke BL: Causes of low peak bone mass in women. Maturitas 111: 61-68, 2018.
12. Heaney RP, Abrams S, Dawson-Hughes B, Looker A, Marcus R, Matkovic V and Weaver C: Peak bone mass. Osteoporos Int 11: 985-1009, 2000.
13. Tønnesen R, Schwarz P, Hovind PH and Jensen LT: Physical exercise associated with improved BMD independently of sex and vitamin D levels in young adults. Eur J Appl Physiol 116: 1297-1304, 2016.
14. Yu Y, Li X, Zheng M, Zhou L, Zhang J, Wang J and Sun B: The potential benefits and mechanisms of protein nutritional intervention on bone health improvement. Crit Rev Food Sci Nutr 64: 6380-6394, 2024.
15. Yuan W, Yang M and Zhu Y: Development and validation of a gene signature predicting the risk of postmenopausal osteoporosis. Bone Joint Res 11: 548-560, 2022.
16. Wang J, Kong C, Pan F and Lu S: Construction and validation of a nomogram clinical prediction model for predicting osteoporosis in an asymptomatic elderly population in beijing. J Clin Med 12: 1292, 2023.
17. Eastell R and Szulc P: Use of bone turnover markers in postmenopausal osteoporosis. Lancet Diabetes Endocrinol 5: 908-923, 2017.
18. Muraca M and Cappariello A: The role of extracellular vesicles (EVs) in the epigenetic regulation of bone metabolism and osteoporosis. Int J Mol Sci 21: 8682, 2020.

19. Ciuffi S, Donati S, Marini F, Palmini G, Luzi E and Brandi ML: Circulating MicroRNAs as novel biomarkers for osteoporosis and fragility fracture risk: Is there a use in assessment risk? Int J Mol Sci 21: 6927, 2020.
20. Lou W, Liu J, Ding B, Chen D, Xu L, Ding J, Jiang D, Zhou L, Zheng S and Fan W: Identification of potential miRNA-mRNA regulatory network contributing to pathogenesis of HBV-related HCC. J Transl Med 17: 7, 2019.
21. Ritchie ME, Phipson B, Wu D, Hu Y, Law CW, Shi W and Smyth GK: limma powers differential expression analyses for RNA-sequencing and microarray studies. Nucleic Acids Res 43: e47, 2015.
22. Love MI, Huber W and Anders S: Moderated estimation of fold change and dispersion for RNA-seq data with DESeq2. Genome Biol 15: 550, 2014.
23. Szklarczyk D, Morris JH, Cook H, Kuhn M, Wyder S, Simonovic M, Santos A, Doncheva NT, Roth A, Bork P, *et al*: The STRING database in 2017: Quality-controlled protein-protein association networks, made broadly accessible. Nucleic Acids Res 45(D1): D362-D368, 2017.
24. Subramanian A, Tamayo P, Mootha VK, Mukherjee S, Ebert BL, Gillette MA, Paulovich A, Pomeroy SL, Golub TR, Lander ES and Mesirov JP: Gene set enrichment analysis: A knowledge-based approach for interpreting genome-wide expression profiles. Proc Natl Acad Sci USA 102: 15545-15550, 2005.
25. Shannon P, Markiel A, Ozier O, Baliga NS, Wang JT, Ramage D, Amin N, Schwikowski B and Ideker T: Cytoscape: A software environment for integrated models of biomolecular interaction networks. Genome Res 13: 2498-2504, 2003.
26. Li HM, Liu Y, Ding JY, Zhang R, Liu XY and Shen CL: In silico analysis excavates a novel competing endogenous RNA subnetwork in adolescent idiopathic scoliosis. Front Med (Lausanne) 7: 583243, 2020.
27. Sauerbrei W, Royston P and Binder H: Selection of important variables and determination of functional form for continuous predictors in multivariable model building. Stat Med 26: 5512-5528, 2007.
28. Iasonos A, Schrag D, Raj GV and Panageas KS: How to build and interpret a nomogram for cancer prognosis. J Clin Oncol 26: 1364-1370, 2008.
29. Pencina MJ and D'Agostino RB: Overall C as a measure of discrimination in survival analysis: Model specific population value and confidence interval estimation. Stat Med 23: 2109-2123, 2004.
30. Vickers AJ and Elkin EB: Decision curve analysis: A novel method for evaluating prediction models. Med Decis Making 26: 565-574, 2006.
31. Mortazavi A, Williams BA, McCue K, Schaeffer L and Wold B: Mapping and quantifying mammalian transcriptomes by RNA-Seq. Nat Methods 5: 621-628, 2008.
32. Tu JB, Liao WJ, Liu WC and Gao XH: Using machine learning techniques to predict the risk of osteoporosis based on nationwide chronic disease data. Sci Rep 14: 5245, 2024.
33. Lee SH, Jeong HM, Han Y, Cheong H, Kang BY and Lee KY: Prolyl isomerase Pin1 regulates the osteogenic activity of Osterix. Mol Cell Endocrinol 400: 32-40, 2015.
34. Piao M, Lee SH, Hwang JW, Kim HS, Han YH and Lee KY. The cell-penetrating peptide GV1001 enhances bone formation via Pin1-Mediated augmentation of Runx2 and osterix stability. Biomolecules 14: 812, 2024.
35. Zhang Y, Shi T and He Y: GPR35 regulates osteogenesis via the Wnt/GSK3β/β-catenin signaling pathway. Biochem Biophys Res Commun 556: 171-178, 2021.
36. Pham TH, Kim EN, Trang NM and Jeong GS: Gallic acid induces osteoblast differentiation and alleviates inflammatory response through GPR35/GSK3β/β-catenin signaling pathway in human periodontal ligament cells. J Periodontal Res 59: 204-219, 2024.
37. Li L, Tang P, Zhou Z, Wang Q, Xu T, Zhao S, Huang Y, Kong F, Liu W, Cheng L, *et al*: GIT1 regulates angiogenic factor secretion in bone marrow mesenchymal stem cells via NF-κB/Notch signalling to promote angiogenesis. Cell Prolif 52: e12689, 2019.
38. Cheng L, Zhou Z, Li Q, Li W, Li X, Li G, Fan J, Yu L and Yin G: Dendronized chitosan hydrogel with GIT1 to accelerate bone defect repair through increasing local neovascular amount. Bone Rep 19: 101712, 2023.
39. Yu Y, Yao P, Wang Z and Xie W: Down-regulation of FTX promotes the differentiation of osteoclasts in osteoporosis through the Notch1 signaling pathway by targeting miR-137. BMC Musculoskelet Disord 21: 456, 2020.
40. Shao JL, Li H, Zhang XR, Zhang X, Li ZZ, Jiao GL and Sun GD: Identification of serum exosomal MicroRNA expression profiling in menopausal females with osteoporosis by high-throughput sequencing. Curr Med Sci 40: 1161-1169, 2020.
41. Ru X, Cai P, Tan M, Zheng L, Lu Z and Zhao J: Temporal transcriptome highlights the involvement of cytokine/JAK/STAT3 signaling pathway in the osteoinduction of BMSCs. J Orthop Surg Res 18: 289, 2023.
42. Marques-Carvalho A, Sardão VA, Kim HN and Almeida M: ECSIT is essential for RANKL-induced stimulation of mitochondria in osteoclasts and a target for the anti-osteoclastogenic effects of estrogens. Front Endocrinol (Lausanne) 14: 1110369, 2023.
43. Chen L, Zhang RY, Xie J, Yang JY, Fang KH, Hong CX, Yang RB, Bsoul N and Yang L: STAT3 activation by catalpol promotes osteogenesis-angiogenesis coupling, thus accelerating osteoporotic bone repair. Stem Cell Res Ther 12: 108, 2021.
44. Zhao X, Zhou J, Liu Y, Wang J, Liu Y, Wang B, Han C, Zhao S and Zhang Y: Puerarin alleviates osteoporosis in rats by targeting the JAK2/STAT3 signaling pathway. Biomol Biomed 24: 1651-1661, 2024.
45. Chen J, Sun Q and Yin W: Th17 cell-related gene biomarkers in osteoporosis: Comprehensive bioinformatics analysis and in vivo validation. Horm Metab Res 56: 373-380, 2024.
46. Zhang B, Zhao J, Yan H, Zhao Y, Tian H, Wang C, Wang R, Jin J, Chen Y, Yang C, *et al*: A novel nano delivery system targeting different stages of osteoclasts. Biomater Sci 10: 1821-1830, 2022.
47. Wang C, Zheng H, He JW, Zhang H, Yue H, Hu WW, Gu JM, Shao C, Fu WZ, Hu YQ, *et al*: Genetic polymorphisms in the mevalonate pathway affect the therapeutic response to alendronate treatment in postmenopausal Chinese women with low bone mineral density. Pharmacogenomics J 15: 158-164, 2015.
48. Chougule A, Zhang C, Vinokurov N, Mendez D, Vojtisek E, Shi C, Zhang J and Gardinier J: Purinergic signaling through the P2Y2 receptor regulates osteocytes' mechanosensitivity. J Cell Biol 223: e202403005, 2024.
49. Wei H, Bi Y, Wang Y, Zhao Q, Zhang R, Li J and Bao J: Serum bone remodeling parameters and transcriptome profiling reveal abnormal bone metabolism associated with keel bone fractures in laying hens. Poult Sci 102: 102438, 2023.
50. Yao XT, Li PP, Liu J, Yang YY, Luo ZL, Jiang HT, He WG, Luo HH, Deng YX and He BC: Wnt/β-Catenin promotes the osteoblastic potential of BMP9 Through down-regulating Cyp26b1 in mesenchymal stem cells. Tissue Eng Regen Med 20: 705-723, 2023.
51. Xing Q, Feng J and Zhang X: Semaphorin3B promotes proliferation and osteogenic differentiation of bone marrow mesenchymal stem cells in a high-glucose microenvironment. Stem Cells Int 2021: 6637176, 2021.
52. Dai M, Hong W and Ouyang Y: Identification and validation of hub genes and construction of miRNA-Gene and transcription factor-gene networks in adipogenesis of mesenchymal stem cells. Stem Cells Int 2024: 5789593, 2024.
53. Hu Y, Han J, Ding S, Liu S and Wang H: Identification of ferroptosis-associated biomarkers for the potential diagnosis and treatment of postmenopausal osteoporosis. Front Endocrinol (Lausanne) 13: 986384, 2022.
54. Gao P, Pan X, Wang S, Guo S, Dong Z, Wang Z, Liang X, Chen Y, Fang F, Yang L, *et al*: Identification of the transcriptome signatures and immune-inflammatory responses in postmenopausal osteoporosis. Heliyon 10: e23675, 2024.
55. Geng Y, Shao R, Xu T and Zhang L: Identification of a potential signature to predict the risk of postmenopausal osteoporosis. Gene 894: 147942, 2024.
56. Zeng R, Ke TC, Ou MT, Duan LL, Li Y, Chen ZJ, Xing ZB, Fu XC, Huang CY and Wang J: Identification of a potential diagnostic signature for postmenopausal osteoporosis via transcriptome analysis. Front Pharmacol 13: 944735, 2022.
57. Schembri M and Formosa MM: Identification of osteoporosis genes using family studies. Front Endocrinol (Lausanne) 15: 1455689, 2024.
58. Elahmer NR, Wong SK, Mohamed N, Alias E, Chin KY and Muhammad N: Mechanistic insights and therapeutic strategies in osteoporosis: A comprehensive review. Biomedicines 12: 1635, 2024.
59. Tang SS, Yin XJ, Yu W, Cui L, Li ZX, Cui LJ, Wang LH and Xia W: Prevalence of osteoporosis and related factors in postmenopausal women aged 40 and above in China. Zhonghua Liu Xing Bing Xue Za Zhi 43: 509-516, 2022 (In Chinese).

60. Tang G, Feng L, Pei Y, Gu Z, Chen T and Feng Z: Low BMI, blood calcium and vitamin D, kyphosis time, and outdoor activity time are independent risk factors for osteoporosis in postmenopausal women. Front Endocrinol (Lausanne) 14: 1154927, 2023.
61. Pouresmaeili F, Kamalidehghan B, Kamarehei M and Goh YM: A comprehensive overview on osteoporosis and its risk factors. Ther Clin Risk Manag 14: 2029-2049, 2018.
62. Ono Y, Miyakoshi N, Kasukawa Y, Akagawa M, Kimura R, Nagahata I, Yuasa Y, Sato C and Shimada Y: Diagnosis of presarcopenia using body height and arm span for postmenopausal osteoporosis. Clin Interv Aging 15: 357-361, 2020.
63. Zeitlin J, Parides MK, Lane JM, Russell LA and Kunze KN: A clinical prediction model for 10-year risk of self-reported osteoporosis diagnosis in pre- and perimenopausal women. Arch Osteoporos 18: 78, 2023.
64. Cheishvili D, Parashar S, Mahmood N, Arakelian A, Kremer R, Goltzman D, Szyf M and Rabbani SA: Identification of an epigenetic signature of osteoporosis in blood DNA of postmenopausal women. J Bone Miner Res 33: 1980-1989, 2018.

Copyright © 2026 Huang et al. This work is licensed under a Creative Commons Attribution-NonCommercial-NoDerivatives 4.0 International (CC BY-NC-ND 4.0) License.